Chaos, Solitons and Fractals 153 (2021) 111416

Contents lists available at ScienceDirect

Chaos, Solitons and Fractals

Nonlinear Science, and Nonequilibrium and Complex Phenomena

journal homepage: www.elsevier.com/locate/chaos

Frontiers

Taming Faraday waves in binary fermionic clouds: The effect of Zeeman interaction

P. Díaz [a], L.M. Pérez [b], L.I. Reyes [b], D. Laroze [b], J. Bragard [c,*]

[a] Departamento de Ciencias Físicas, Universidad de La Frontera, Casilla 54-D, Temuco, Chile
[b] Instituto de Alta Investigación, CEDENNA, Universidad de Tarapacá, Casilla 7D, Arica, Chile
[c] Departamento de Física y Matemática Aplicada, Universidad de Navarra, Pamplona, 31080, Spain

ARTICLE INFO

Article history:
Received 11 August 2021
Accepted 29 August 2021

Keywords:
Cold atoms
Fermi-Fermi mixtures
Faraday waves

ABSTRACT

This work presents a study of the Faraday instability in a parametrically forced Fermi-Fermi mixture. The condensate is confined in the transversal spatial dimension with a strong parametric confinement potential and in the longitudinal spatial dimension with a weaker potential. The theoretical description is done using the mean-field theory with two amplitude equations that represent each spin state. In order to stabilize the Faraday patterns, a phenomenological damping term is introduced. The influence of the Zeeman interaction is analyzed in detail. In particular, phase diagrams of the existence and stability of the Faraday waves are calculated as a function of the Zeeman interaction, the coupling parameter, and the forcing amplitude. The degree of segregation of the two fields and their synchronization level is also calculated as a function of the Zeeman parameter. In addition, we examine how the pattern wavelength varies as a function of the Zeeman parameter and the forcing frequency.

1. Introduction

In recent years, the field of ultracold fermionic atoms has generated many interesting investigations, both in the experimental and theoretical domains. Of particular interest, one can cite the problems related to their confined geometry, their size, and the interaction strength that can be manipulated in a considerable range [1–5].

The main objective pursued by this new branch of the Solid State Physics is to have the possibility to manipulate systems in μm - scale with macroscopically confined potentials, such as optical lattices or magnetic traps, with *Bosonic* and/or *Fermionic* behaviors. For instance, the determination of phase diagrams of the quasi-one-dimensional Fermi system described by the many-body Hamiltonian model has been analyzed in-depth and various situations [6–13]. The mean-field theory applied to low dimensional Fermi superfluid or Fermi mixtures has been developed recently [14–22].

Moreover, studies focusing on the nonlinear dynamics of the ultra-cold degenerate quantum gases are now growing in the literature; for example, one can cite, without being exhaustive, the generation of different types of vortex rings [23–25], shock waves [26,27] or chaotic dynamics [28], just to mention a few. In addition, the inclusion of the Zeeman term in binary Bose-Einstein condensates has allowed to generate gap of solitons when the spin-orbit coupling between spin states is considered [29–31], which shows the potential that entails the symmetry breaking generated by the Zeeman term by unbalancing the number of particles per spin state. Recently, a study on soliton in binary fermionic clouds in the free space was analyzed [32]. Interesting review articles about the nonlinear manifestation in degenerate quantum gases are to be found in References [33–35].

In several situations, the non-equilibrium fermionic atoms are maintained out of equilibrium by employing an external forcing. This forcing can be constant or time-dependent. In time-dependent forcing, one can add the modulation of at least one parameter of the system under study. This type of energy injection is traditionally denominated parametric forcing. For a parametrically driven system, resonance occurs at a different frequency than that of the forcing frequency; these classes of systems are currently topic of interest [36–44].

The most well-known example of parametric instabilities is the celebrated Faraday instability. Faraday discovered this instability in a seminal work back in 1831 [45]. In his setup, a liquid is contained in a vessel subjected to vertical oscillations. In this fluid system,

* Corresponding author.
E-mail address: jbragard@unav.es (J. Bragard).

https://doi.org/10.1016/j.chaos.2021.111416

the observed pattern oscillates at half of the driving frequency [45]. Subsequently, this universal phenomenon has been studied extensively in the literature [46–49]. For example, the Faraday waves (FWs) were observed in Bose-Einstein Condensates (BEC) [50–52]. The authors have shown that periodically modulating the transverse confinement and thus the nonlinear interaction in the BEC, excites small amplitude longitudinal oscillation through a parametric resonance. This observed effect was predicted a few years earlier, using as a theoretical model, i.e., the parametrically driven Gross-Pitaevskii equation [53,54]. More recently, the existence of FWs was also predicted in a parametrically forcing elongated superfluid fermionic cloud, using the framework of the superfluid hydrodynamics [55]. Further works on FWs in several ultra-cold systems can be found in Refs. [56–62].

This work aims at studying the Faraday waves that occur in a parametrically driven elongated binary fermionic cloud. The parametrical forcing is applied in the transverse spatial dimension, while a weak confinement potential is established in the longitudinal dimension. We use a theoretical description in the continuum framework for a one-dimensional, extended system. This description ensues from a mean-field theory, also taking into account the non-variational term. In particular, the dissipation effects are introduced in an ad-hoc manner by the inclusion of a phenomenological damping coefficient [53,54,63,64]. Note that it was applied in the same way by Arecchi et al. in the study of an open Bose system [65].

The nonlinear term related to the fermion-fermion interaction is the standard cross cubic one, such that its coefficient has been chosen as a time-dependent function. In addition, the Zeeman interaction has been addressed, showing that the term can modify the onset and the stability of the Faraday waves. In particular, we have computed the phase diagrams on the existence of the FW and the degree of synchronization of the fermionic fields as a function of the Zeeman parameter and the static coupling coefficient. Finally, we show the influence of the driven frequency on the waves, as well. The paper is arranged in the following manner: In Section 2, the theoretical model is presented. In Section 3, parametric instabilities are numerically studied. Finally, the conclusions are drawn in Section 4.

2. Theoretical model

The model consists of the coupling of two fermionic fields through two nonlinear Schrödinger equations [19], valid within the framework of the mean-field theory. The two components represent the spin-up and spin-down atomic states. The fields interact through a cubic interaction term that describes the dispersion between species. The fermionic mixture is immersed in a quadratic potential to confine the gas in a region of space (around $z = 0$). The longitudinal potential (in the z direction) is far weaker than the potential used for the transverse confinement. The confinement potential in the transverse plane possesses a cylindrical symmetry. In such a setting, we can use the reduced formalism of the one-dimensional nonlinear Schrödinger equations [21,22]. Also, let us comment that the interaction among the spin states is described through the effective Pauli nonlinearity [32].

It has been shown previously that for a bosonic condensate, if oscillations are induced on the transverse trapping potential, then for some parameter values, Faraday waves are elicited [50–54]. In the hydrodynamic description for fermions, one also expects Faraday waves [55]. However, these waves are unstable if only energy injection is considered. For stabilizing the Faraday waves, it is necessary to include dissipation. In the present paper, we will use the technique introduced by Arecchi et al. to include the dissipation term [65] $\Gamma = (1 - i\gamma)$, where γ is a dimensionless phenomenological dissipation parameter.

In this framework, the Fermi-Fermi mixture can be described by the following set of dimensionless equations:

$$i\partial_t \psi_1 = \Gamma\left[-\partial_z^2 + V_1 + \epsilon\right]\psi_1 + \Gamma\left[\frac{\pi^2}{4}n_1^2 + g_{12}n_2\right]\psi_1 \tag{1}$$

and

$$i\partial_t \psi_2 = \Gamma\left[-\partial_z^2 + V_2 - \epsilon\right]\psi_2 + \Gamma\left[\frac{\pi^2}{4}n_2^2 + g_{12}n_1\right]\psi_2, \tag{2}$$

where ψ_1 and ψ_2 are the fermionic fields of the two spin states, such that $n_1 = |\psi_1|^2$ and $n_2 = |\psi_2|^2$ correspond to the number density of the two states, respectively. Besides, we denote the "weak" harmonic confinement potential in the longitudinal direction z, for both species, by:

$$V_1(z) = V_2(z) = \frac{1}{2}\omega_z^2 z^2, \tag{3}$$

which is needed to ensure the confinement of the gas in a determined spatial region (around $z = 0$). Due to the different spin states, the Zeeman interaction comes in equations (1) - (2) through the ϵ term. Note that this term is not necessarily small and it depends on the applied magnetic field.

The coupling coefficient, g_{12}, depends linearly on the transverse confinement, which in turn is proportional to the transverse magnetic field with cylindrical symmetry, which allows treating the gases in a single spatial dimension (z). Experimentally, it is possible to generate oscillations in the interaction parameters by varying this cross-sectional field, producing a time-dependent coefficient $g_{12}(t)$ [50]. This effect induces parametric instabilities. Here, we consider the following time dependence for the coupling coefficient:

$$g_{12}(t) = g_{12,0}(1 + p\cos(\Omega t)), \tag{4}$$

where $p \leq 1$ is a dimensionless parameter that quantifies the amplitude of the oscillations of the transverse confinement field and Ω represents the forcing frequency.

Note that in Eqs. (1-2), we have the constraint that the total number of particles,

$$N = \int (n_1 + n_2)dz, \tag{5}$$

is constant. Finally, let us comment that to characterize the different dynamical regimes, we will use the Fourier power spectrum of the temporal signal, i.e., $|\mathfrak{F}_h(\omega)|^2$, where $\mathfrak{F}$ is the Fourier transform of the temporal function $h(\tau)$,

$$\mathfrak{F}_h(\omega) = \frac{1}{\sqrt{2\pi}}\int_0^{\tau_{\max}} h(\tau)\exp(-i\omega\tau)d\tau. \tag{6}$$

If the time series is regular, $|\mathfrak{F}_h(\omega)|^2$ has a finite number of quasi-discrete peaks. On the contrary, the power spectrum is essentially continuous and the original time series is chaotic [66].

3. Numerical simulations

In this section, we will characterize the Faraday waves displayed in Fig. 1. Due to the large number of parameters, we have first set the dissipation parameter to $\gamma = 0.05$, the confined potential coefficient is set to $\omega_z = 0.1$, and the total number of particles is fixed to $N = 200$. For most of the simulations the forcing frequency is taken at $\Omega = 10$. The numerical simulations of Eqs. (1-2) have been performed using the standard fourth-order Runge-Kutta algorithm and a second-order centered finite differences for space discretization. The numerical parameters are $\Delta\tau = 0.0025$ and $\Delta x = 0.1$ in a box of size $L = 120$ in dimensionless units. The convergence of the numerical simulations was checked by reproducing some results with smaller grid values of $\Delta\tau$ and Δx and

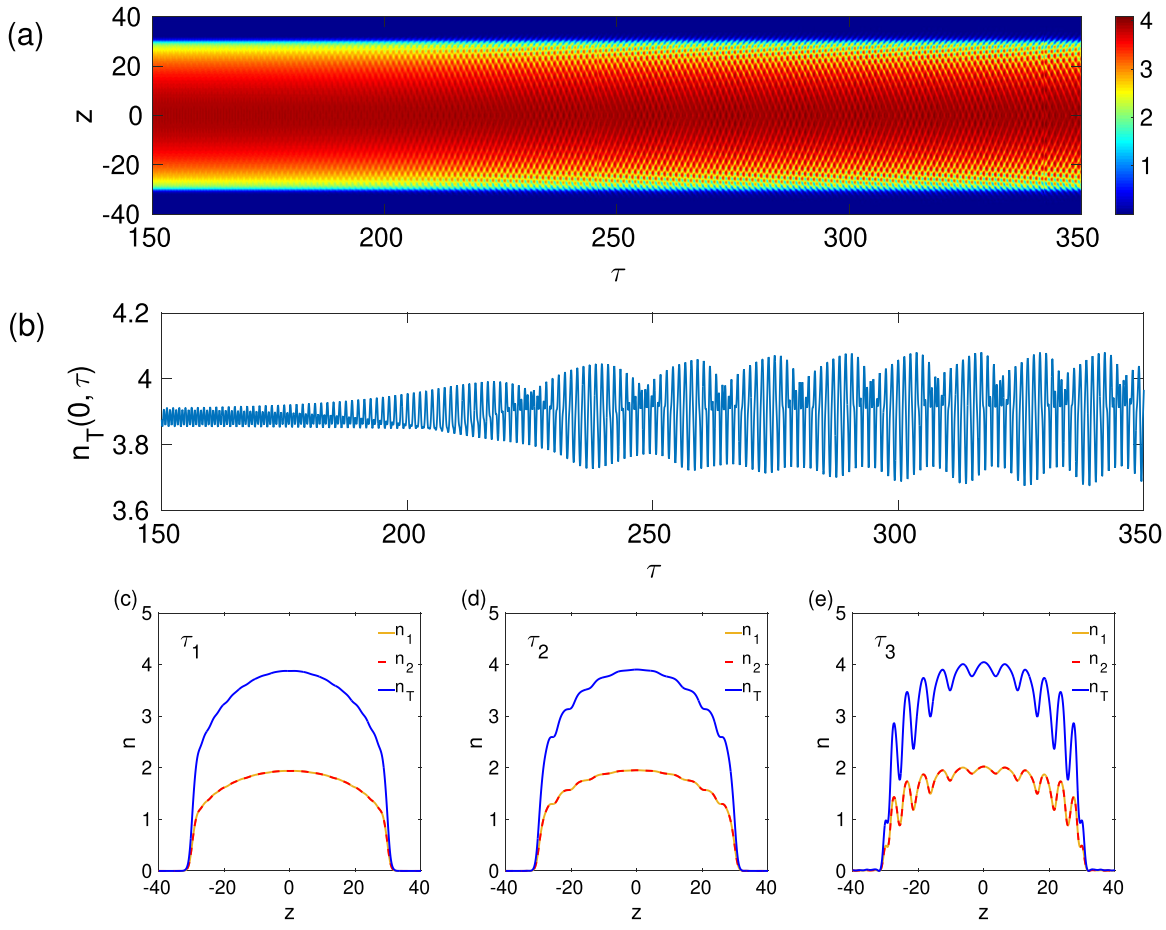

Fig. 1. Faraday pattern formation in a binary Fermi condensate. Here the Zeeman interaction term is set to $\epsilon = 0.0$. (a) The top panel depicts the space-time evolution of the total density $n_T = n_1 + n_2$ showing the appearance of the Faraday pattern. (b) Time evolution of the total density n_T measured at $z = 0$. Lower panels are displaying the density profiles at different times: (c) $\tau_1 = 150$, (d) $\tau_2 = 180$ y (e) $\tau_3 = 340$. Parameters for this simulation were set to: $\Omega = 10$, $\omega_z = 0.1$, $\gamma = 0.05$, $p = 1$ and $g_{12,0} = -2.82$. We measure that the Faraday wavelength is approximately $\lambda_F = 5.48$ as shown in panel (e). Note that the spacing is not constant.

with different sizes of the integration domain L. All quantities presented in this manuscript have been computed as averages over ten independent realizations of random initial conditions.

Panel (a) in Fig. 1 reveals that the total density, $n_T(\tau, z)$, becomes unstable and develop a Faraday wave pattern. We clearly observe the transient states prior to the formation of the Faraday waves. Panel (b) in Fig. 1 shows the total density time series for the central point at $z = 0$. In this case, the transient lasts approximately $\tau \approx 300$. Panels (c) - (e) in Fig. 1 display some snapshots of the spatial density profiles of each spin state n_1, n_2, as well as the total density n_T at three different times, i.e., $\tau = (150, 180, 340)$, respectively. The first two profiles are in the transient phase, while for $\tau = 340$, the characteristic oscillatory pattern of the Faraday wave is clearly seen. From Panel (e) in Fig. 1 we measure an approximate wavenumber of $k_F = (2\pi)/\lambda_F \approx 1.15$. Let us remind that we have set the Zeeman parameter in Fig. 1 to $\epsilon = 0$. We will look at the influence of such a parameter in the following subsection.

3.1. Zeeman effect

We expect a noticeable influence of the Zeeman term on the stability and dynamics of the Faraday wave pattern observed in Fig. 1. In this section, we will study the influence of the Zeeman term by setting several different values of the parameter ϵ in the simulations of Eqs. (1-2).

To avoid spurious results due to transient behaviors, signals corresponding to $6 \times 10^3 \times (2\pi/\Omega)$ initial time units are discarded in the following simulations. Then, after the transient has elapsed, the signal is acquired for $10^2 \times (2\pi/\Omega)$ time units.

Left panels of Fig. 2 display the space-time evolutions of the total density for different values of the Zeeman parameter. We have set the parameter ϵ to (4,2,0) from the top to the bottom panels in Fig. 2. We can observe that when $\epsilon = 4$, the system exhibits a very ordered Faraday pattern. On the contrary, when the splitting parameter value is reduced, the pattern becomes disordered until it reaches a chaotic state when $\epsilon = 0$. This transition is also observed through the power spectra of the total density taken at the central point, $A_{n_T}(\omega) = |\mathfrak{F}_{n_T(z=0)}(\omega)|^2$, as shown in the right column panels of Fig. 2. Indeed, in panel (b), we observe that the frequency associated with the maximum power is $\Omega/2$, which is the characteristic value for the parametric instabilities. In contrast, in panel (f), a continuum of frequencies is observed in the power spectrum typical of spatiotemporal chaos and the Faraday waves are unstable.

Fig. 3 displays a phase diagram of the stability of the Faraday waves as a function of the parameters $g_{12,0}$ and ϵ. We observe three separated regimes. The first regime, in the upper right corner in Fig. 3 corresponds to oscillations that do not develop a spatial pattern (background oscillations). The second regime corresponds to the Faraday waves that are stable in a range of values given in Fig. 3. Finally, there is a region below the (red) dashed-square line

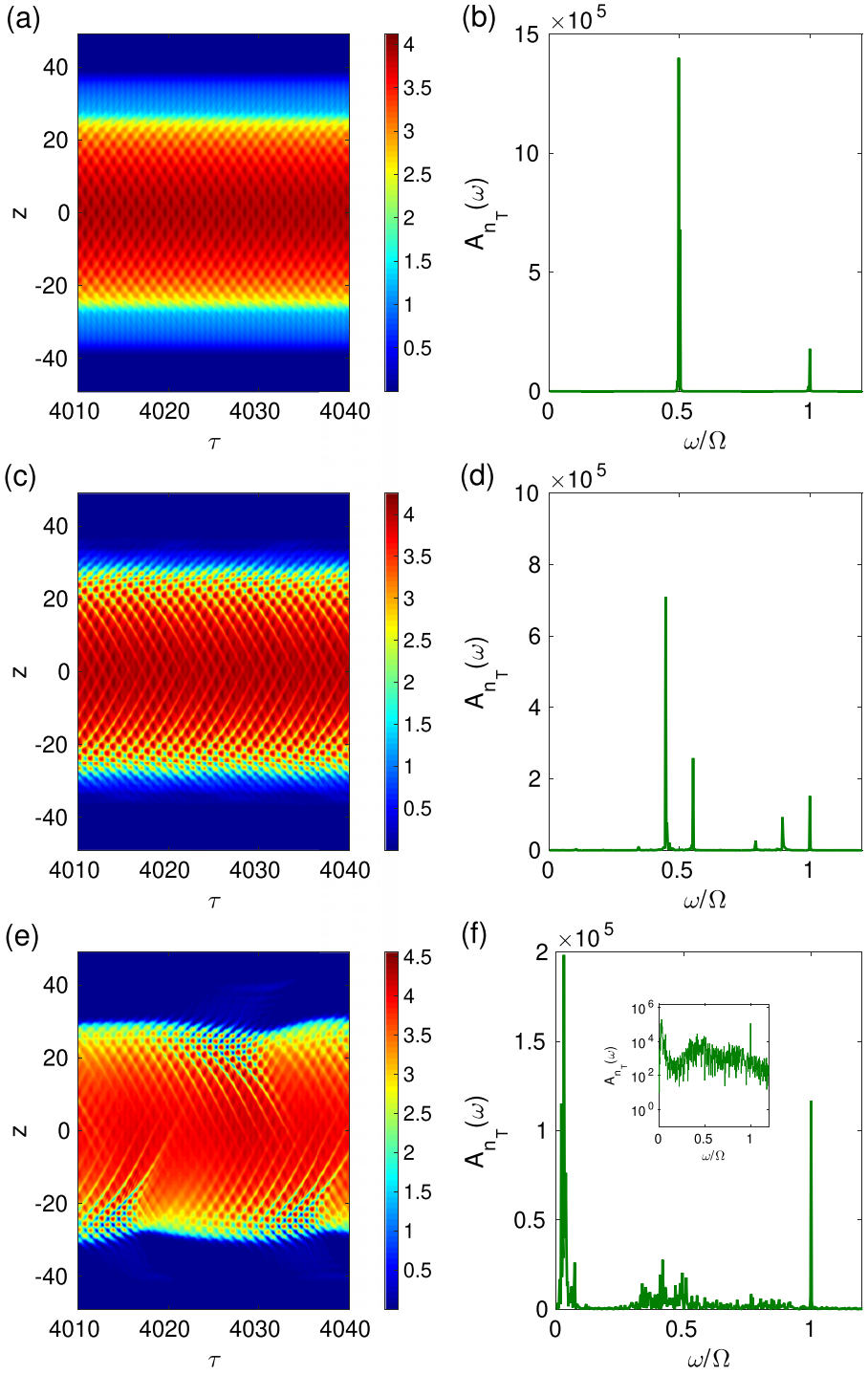

Fig. 2. Influence of the Zeeman interaction term on the stability of the Faraday pattern. From top to bottom, we have set the parameter to $\epsilon = 4.0$, $\epsilon = 2.0$ and $\epsilon = 0.0$. The left panels correspond to the space-time evolutions of the total density. The right panels correspond to the power spectra of the FFT for the central ($z = 0$) time evolution total density n_T. In the simulations, we have set $g_{12,0} = -3.23$, and the rest of the parameters are fixed as in Fig. 1.

in Fig. 3 where the Faraday waves experience a secondary bifurcation, and the resulting regime is chaotic. The phase diagram shown in Fig. 3 was computed using the Fourier power spectrum of the total density as a tool to determine the pattern.

Let us now characterize the dependence of the Faraday wavelength pattern λ_F as a function of the Zeeman splitting parameter ϵ as shown in Fig. 4. Again, to calculate this wavelength, we will use the Fourier transform. This time we will use the spatial version of the FFT. We evaluate λ_F by following these steps: first, we subtract from the total density, n_T, its time average,

$$\Delta(z,\tau) = n_T(z,\tau) - < n_T(z,\tau) >_\tau,$$

which produces a spatiotemporal pattern of zero mean. Secondly, we evaluate the spatial Fourier spectrum of Δ at different times,

$$S_\Delta(k,\tau) = \frac{1}{\sqrt{2\pi}} \int_{-\bar{L}/2}^{+\bar{L}/2} \Delta(z,\tau) \exp(-ikz) dz, \tag{7}$$

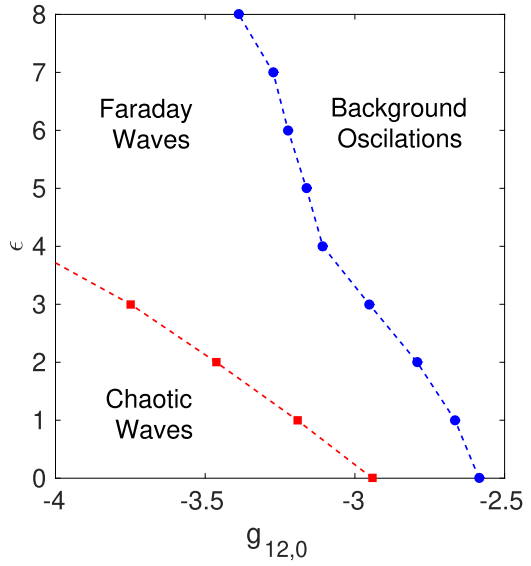

Fig. 3. Phase diagram showing the stability of Faraday waves as a function of $g_{12,0}$ and ϵ. Here, we have set $p = 1$, and the rest of the parameters are fixed as in Fig. 1.

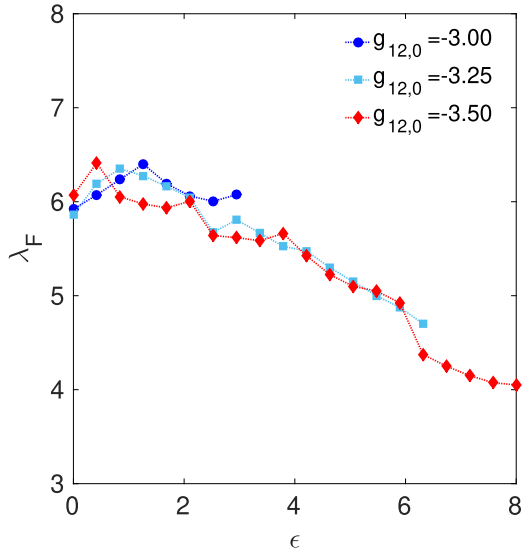

Fig. 4. Dependence of the Faraday wavelength, λ_F as a function of ϵ for three distinct values of $g_{12,0}$: −3 (blue dot symbols); −3.25 (cyan square symbols); −3.50 (red diamond symbols). The rest of the parameters are set to the same values as in Fig. 1. (For interpretation of the references to colour in this figure legend, the reader is referred to the web version of this article.)

where $\bar{L}$ is the system size in which the pattern is confined. We record $|S_\Delta(k,\tau)|^2$ in intervals of every 0.05 unit of time, and then we calculate the temporal average, $< S_\Delta >_\tau$, which is a function only of $\lambda = 2\pi/k$. Finally, we determine for which specific wavelength this temporal average spectrum shows the highest peak in the FW regime. This peak is generally much larger than any others. This procedure gives an approximate value for λ_F extracted from the space-time plot. Fig. 4 shows λ_F as a function of ϵ for three different values of $g_{12,0}$. We observe that when the Zeeman parameter increases, the wavelength decreases globally but in a non-monotonous fashion. We note that the wavelength is not sensitive to the values of the interaction between the fields $g_{12,0}$. However, the range of existence of the FW is sensitive to the coupling parameter. One notes that it increases when the coupling value is decreased.

Because we have two interacting fields, it is natural to ask if this interaction leads to a synchronized state between the two fields. The natural way to characterize such a synchronized state is to compute the Pearson coefficient,

$$C_P = \frac{\langle \delta_1 \delta_2 \rangle_{z,\tau}}{\sqrt{\langle {\delta_1}^2 \rangle_{z,\tau} \langle {\delta_2}^2 \rangle_{z,\tau}}}, \tag{8}$$

which serves as an indicator for complete synchronization [67–70]. In Eq. (8), the symbol δ_j means $\delta_j = n_j - \langle n_j \rangle_{z,\tau}$ and $\langle\ \rangle_{z,\tau}$ denotes the space-time average of the corresponding variables. The Pearson coefficient varies in the range [-1,1], and values close to one indicate complete synchronization while vanishingly small values indicate the lack of synchronization.

Panel (a) of Fig. 5 shows the Pearson coefficient, C_p, as a function of the coupling parameter, $g_{12,0}$, for several values of the Zeeman parameter, ϵ. We notice that the level of synchronization between the fields decreases when the splitting parameter increases. When $\epsilon = 0$, the system is always synchronized regardless of the coupling parameter. This changes as the value of Zeeman grows. In fact, for small and intermediate values of ϵ, we notice that C_p decreases smoothly when the coupling increases. For large values of the splitting Zeeman, the synchronization decays until values of C_p close to 0.6.

Another information is given in panel (b) of Fig. 5, where the ratio between field densities, N_2/N_1, is shown as a function of the coupling parameter, $g_{12,0}$, for the same fixed values of ϵ as in Panel (a) of Fig. 5. We note that the ratio N_2/N_1 increases when ϵ increases. For a fixed value of ϵ, the ratio N_2/N_1 of the two field populations is growing as a function of the coupling parameter. In summary, large values of the coupling parameter, $g_{12,0}$ (in absolute value) and small Zeeman parameter, ϵ are key to maintain the two fields completely synchronized.

Fig. 6 illustrates the influence of the Zeeman parameter on the degree of synchronization and segregation between the two interacting fields. Figs. 6 (a, b) correspond to $\epsilon = 1.0$ and we observe that the two fields are synchronized. The value of the Pearson coefficient is computed and is $C_P \approx 1$. On the contrary, Figs. 6 (c, d) show two decoupled fields and both C_P and N_2/N_1 are no longer close to one. In the lower panels of Fig. 6, the space-time evolution of the individual densities does not have the same color scale. The Faraday wave pattern is observed at the same time that unsynchronized states are also observed.

3.2. Influence of the driving parameters

Fig. 7 depicts a phase diagram for the existence of the Faraday wave as a function of the coupling parameter $g_{12,0}$ and the modulation amplitude p. This diagram is drawn with three different values of the Zeeman parameter, i.e., $\epsilon = (0, 2, 4)$. We observe that for $p < .6$, only background oscillations are possible. The amplitude of the perturbation is not large enough to elicit the Faraday waves. Fig. 7 also reveals and that for larger values of the interaction $g_{12,0}$ (in absolute values), smaller values of p are needed for showing the existence of FW. Also apparent from Fig. 7 is that when the Zeeman parameter increases, the domain of existence of the FW is shrunk.

To end up with the exploration of the coupled fermionic fields, we study the effect of the forcing frequency, Ω, on the Faraday waves occurrence. Fig. 8 shows how the wavelength λ_F varies as a function of Ω for different values of the Zeeman splitting parameter. We can observe that the wavelength is a decreasing function of the forcing frequency Ω. However, the decay is not strictly monotonous. Indeed, the decrease of the wavelength happens in a staggered fashion. The latter is presumably due to the finite size of the system and the influence of the boundary conditions. Also, at

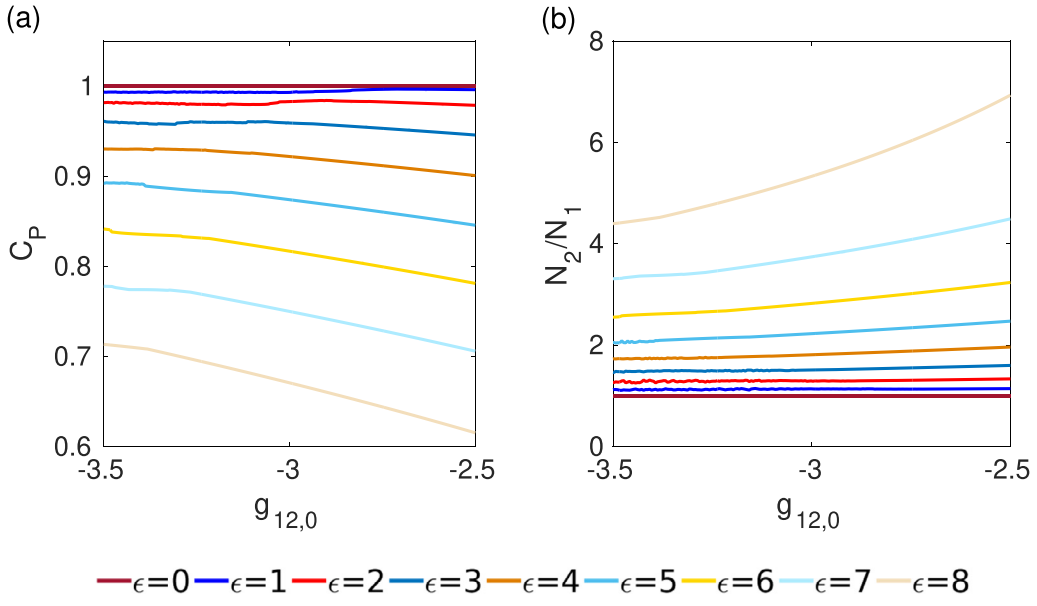

Fig. 5. Influence of the Zeeman parameter ϵ on the synchronization and segregation of the two fields. Panel (a): Pearson coefficient as an indicator of complete synchronization between the two fields as a function of the coupling coefficient $g_{12,0}$ for several values of ϵ (see color code). Panel (b): ratio of the particle densities N_2/N_1 of the two spin states as a function of the coupling coefficient $g_{12,0}$. The rest of the parameters are fixed as in Fig. 1.

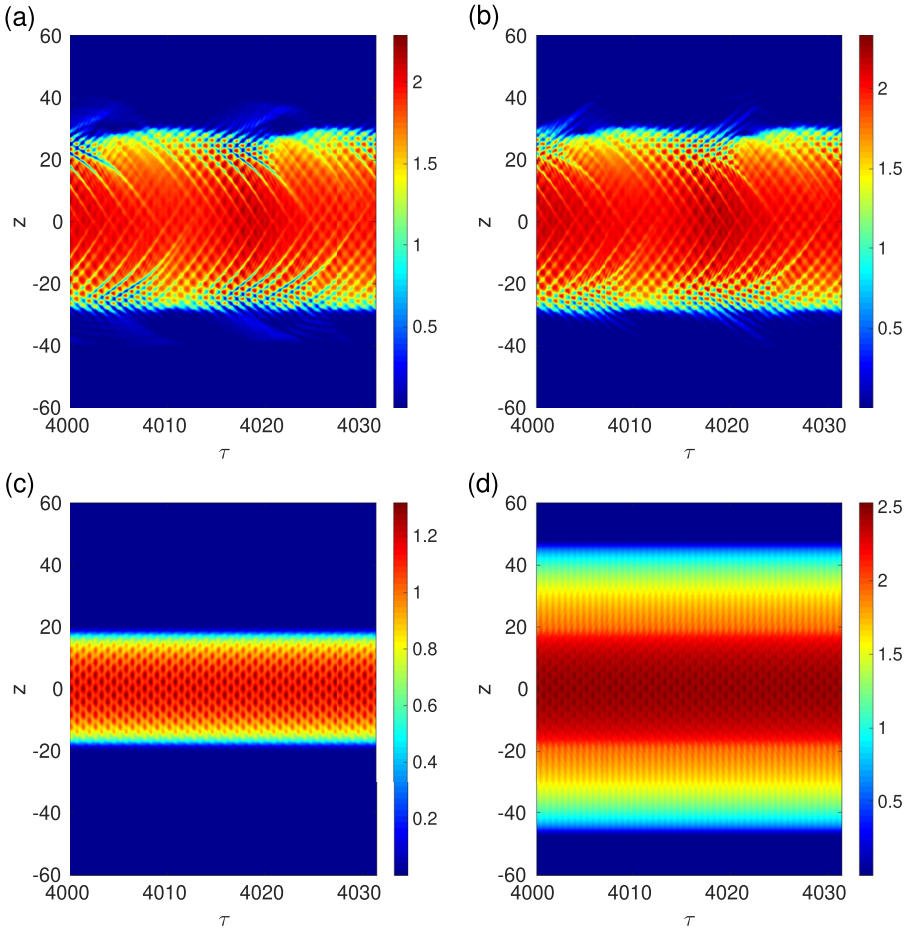

Fig. 6. Space-time evolution of the individual densities n_1 (left panels) and n_2 (right panels). The upper row corresponds to $\epsilon = 1.0$ and a synchronized state ($C_P \approx 1$). The lower row corresponds to $\epsilon = 6.0$, the two fields are not synchronized ($C_P \approx 0.7$). Here we have set $g_{12,0} = -3.4$ and the rest of the parameters are fixed as in Fig. 5.

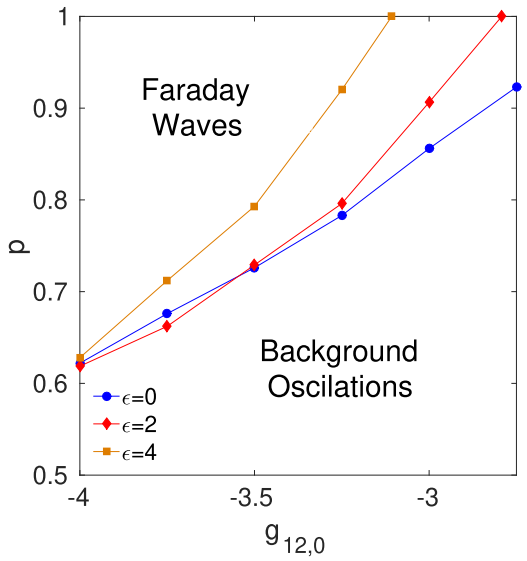

Fig. 7. Influence of the modulation amplitude p on the Faraday wave stability. Phase diagram in the plane $\{g_{12,0}, p\}$ where the Faraday wave are elicited. Three values of ϵ are considered: (0, 2, 4). The rest of the parameters are fixed as in Fig. 1.

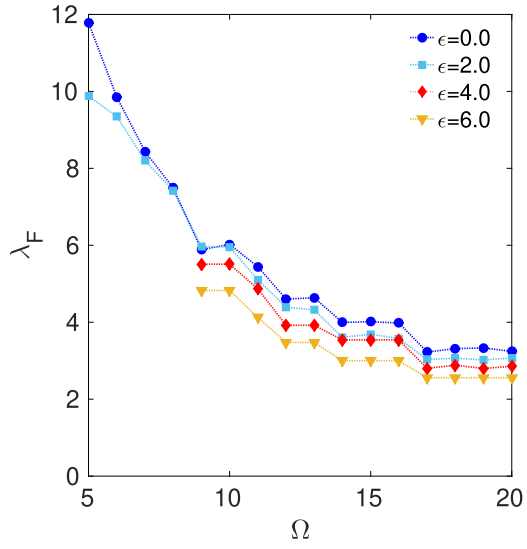

Fig. 8. Dependence of the Faraday wavelength λ_F as a function of the forcing frequency Ω. Four values of ϵ are considered: (0, 2, 4, 6). Here we set $p = 1$ and $g_{12,0} = -3.25$ and the rest of the parameters are fixed as in Fig. 1.

a fixed forcing frequency, when ϵ increases, the wavelength decreases. This could be explained easily with the following argument. When the magnetic field increases, the confined spatial region of the wave becomes narrower, and therefore the associated length is reduced. From Fig. 8, we also remark that the range of existence for the FWs is somewhat reduced for higher values of the Zeeman parameter.

4. Conclusions

Faraday waves have been shown to exist in a binary Fermi mixture. This paper has studied them using numerical simulations in the mean-field approximation in one spatial dimension. Dissipation has been introduced through a non-variational term. The parametric forcing has been included in the effective nonlinear coupling parameter, which is the standard way compatible with the experiments.

A novelty of our study of Faraday waves in cold gases is the introduction of the Zeeman interaction. The influence of the Zeeman interaction parameter on the existence and stability of the FW has been investigated. We have observed that the Zeeman parameter helps in stabilizing the FW. Another conclusion is that the FW wavelength becomes shorter when increasing the Zeeman interaction. In addition, an increase in the Zeeman parameter causes the fields to desynchronize by introducing a symmetry breaking in the density of the spin states. The region of existence of the waves was computed as a function of several system parameters, showing different phase diagrams.

Finally, we have also shown that the forcing frequency modifies the stability region of the FW and their wavelength drastically.

As a future task, we plan to analyze the generation of Faraday waves in higher spatial dimensions with other kinds of potential confinements.

Declaration of Competing Interest

None.

Acknowledgments

JB is truly grateful to the late Prof. Arecchi for hosting him in his Laboratory during a postdoctoral stay at the National Institute of Optics (Florence) in the years 1997 and 1998, where he had the chance to work directly with him and some of his outstanding collaborators. PD, LMP, and DL acknowledge partial financial support from FONDECYT 1180905. DL acknowledges the partial financial support from Centers of excellence with BASAL/CONICYT financing, Grant AFB180001, CEDENNA. JB acknowledges the financial support by MICINN (Spain) through Grant No. SAF-1021 2017-88019-C3-2-R.

References

[1] Giorgini S, Pitaevskii LP, Stringari S. Rev Mod Phys 2008;80:1215.
[2] Bloch I, Dalibard J, Zwerger W. Rev Mod Phys 2008;80:885.
[3] Baumann K, Guerlin C, Brennecke F, Esslinger T. Nature 2010;464:130.
[4] Zipkes C, Ratschbacher L, Palzer S, Sias C, Köhl M. J Phys: Conf Ser 2011;264:012019.
[5] Perron JK, Kimball MO, Mooney KP, Gasparini FM. Nat Phys 2010;6:499.
[6] Lieb EH, Liniger W. Phys Rev 1963;130:1605.
[7] Lieb EH. Phys Rev 1963;130:1616.
[8] Gaudin M. Phys Lett A 1967;24:55.
[9] Yang CN. Phys Rev Lett 1967;19:1312.
[10] Fuchs JN, Recati A, Zwerger W. Phys Rev Lett 2004;93:090408.
[11] Hu H, Liu XJ, Drummond PD. Phys Rev Lett 2007;98:070403.
[12] Giraud S, Combescot R. Phys Rev A 2009;79:043615.
[13] Blume D, Rakshit D. Phys Rev E 2009;80:013601.
[14] Das KK. Phys Rev Lett 2003;90:170403.
[15] Salasnich L. J Math Phys 2000;41:8016.
[16] Salasnich L, Pozzi B, Parola A, Reatto L. J Phys B 2000;33:3943.
[17] Adhikari SK. Phys Rev A 2005;72:053608.
[18] Adhikari SK. Phys Rev A 2006;73:043619.
[19] Adhikari SK. Phys Rev A 2007;76:053609.
[20] Adhikari SK, Malomed BA. Phys Rev A 2006;74:053620.
[21] Salasnich L, Adhikari SK, Toigo F. Phys Rev A 2007;75:023616.
[22] Adhikari SK, Salasnich L. Phys Rev A 2007;76:023612.
[23] Anderson BP, Haljan PC, Regal CA, Feder DL, Collins LA, Clark CW, Cornell EA. Phys Rev Lett 2001;86:2926.
[24] Ginsberg NS, Brand J, Hau LV. Phys Rev Lett 2005;94:040403.
[25] Shomroni I, Lahoud E, Levy S, Steinhauer J. Nat Phys 2009;5:193.
[26] Dutton Z, Budde M, Slowe C, Hau LV. Science 2001;293:663.
[27] Chang JJ, Engels P, Hoefer MA. Phys Rev Lett 2008;101:170404.
[28] Ott H, Fortägh J, Kraft S, Gunther A, Komma D, Zimmermann C. Phys Rev Lett 2003;91:040402.
[29] Sakaguchi H, Malomed BA. Phys Rev A 2018;97:013607.
[30] Kartashov YV, Torner L, Modugno M, Sherman EY, Malomed BA, Konotop VV. Phys Rev Research 2020;2:013036.
[31] Zezyulin DA, Driben R, Konotop VV, Malomed BA. Phys Rev A 2013;88:013607.
[32] Díaz P, Laroze D, Ávila A, Malomed BA. Commun Nonlinear Sci Numer Simulat 2019;70:372.
[33] Physica D, Garcia VM, Berloff NG, Kevrekidis PG, Konotop VV, Malomed BA. An special issue concernig on nonlinear phenomena in degenerate quantum gases

was recently published in. The main references are included in the introductory article: Perez Physica D 2009;238:1289.
[34] Bagnato VS, Frantzeskakis DJ, Kevrekidis PG, Malomed BA, Mihalache D. Rom Rep Phys 2015;67:5.
[35] Dumitru M. Rom Rep Phys 2017;69:403.
[36] Barashenkov IV, Zemlyanaya EV. Phys Rev Lett 1999;83:2568.
[37] Clerc MG, Coulibaly S, Laroze D. Phys Rev E 2008;77:056209.
[38] Clerc MG, Coulibaly S, Laroze D. Int J of Bif Chaos 2009;19:2717.
[39] Clerc MG, Coulibaly S, Laroze D. Int J of Bif Chaos 2009;19:3525.
[40] Clerc MG, Coulibaly S, Laroze D. Physica D 2010;239:72.
[41] Clerc MG, Coulibaly S, Laroze D. EPL 2010;90:38005.
[42] Clerc MG, Coulibaly S, Laroze D. Europhys Lett 2012;97:30006.
[43] Cabanas AM, et al. Chaos, Solitons & Fractals 2021;146:110880.
[44] Cabanas AM, et al. Chaos, Solitons & Fractals 2021;151:111089.
[45] Faraday M. Philos Trans R Soc London 1831;121:299.
[46] Miles JW. J Fluid Mech 1984;148:451.
[47] Wu J, Keolian R, Rudnick I. Phys Rev Lett 1984;52:1421.
[48] Zhang W. Viñals J Phys Rev Lett 1995;74:690.
[49] Wang X, Wei R. Phys Rev E 1998;57:2405.
[50] Engels P, Atherton C, Hoefer MA. Phys Rev Lett 2007;98:095301.
[51] Wille E, Spiegelhalder FM, Kerner G, Naik D, Trenkwalder A, Hendl G, Schreck F, Grimm R, Tiecke TG, Walraven J TM, Kokkelmans S, JMF J, Tiesinga E, Julienne PS. Phys Rev Lett 2008;100:053201.
[52] Nicolin AI, Carretero-Gonzlez R, Kevrekidis PG. Phys Rev A 2007;76:063609.
[53] Staliunas K, Longhi S, Valcárcel GJ. Phys Rev Lett 2002;89:210406.
[54] Staliunas K, Longhi S, de Valcárcel GJ. Phys Rev A 2004;70. 011601(R)
[55] Capuzzi P, Vignolo P. Phys Rev A 2008;78:043613.
[56] Nicolin AI, Raportaru MC. Physica A 2012;389:4663.
[57] Nicolin AI. Phys Rev E 2011;84:056202.
[58] Balaz A, Nicolin AI. Phys Rev A 2012;85:023613.
[59] Balaz A, Paun R, Nicolin AI, Balasubramanian S, Ramaswamy R. Phys Rev A 2014;89:023609.
[60] Vudragovic D, Balaz A. Symmetry-Basel 2019;11:1090.
[61] Abdullaev FK, Gammal A, Kumar RK. Tomio J Phys B 2019;52:195301.
[62] Fang L, Shujin D, Liang Z, Jiahui X, Licheng Y, Haibin W. Sci China Phys Mech 2021;64:294212.
[63] Pitaevskii LP. Sov Phys J ETP 1959;35:282.
[64] Choi S, Morgan SA, Burnett K. Phys Rev A 1998;57:4057.
[65] Arecchi FT, Bragard J, Castellano LM. Opt Commun 2000;179:149.
[66] Ott E. Chaos in dynamical systems. Cambridge: Cambridge University Press; 1993.
[67] Boccaletti S, Kurths J, Osipov G, Valladares DL, Zhou CS. Phys Reports 2002;366:1.
[68] Boccaletti S, Bragard J, Arecchi FT, Mancini H. Phys Rev Lett 1999;83:536.
[69] Bragard J, Arecchi FT, Boccaletti S. Int J of Bif and Chaos 2000;10:2381.
[70] Bragard J, Boccaletti S, Arecchi FT. Int J of Bif and Chaos 2001;11:2715.